

Article

# Non-Symmetrically Fused Bis(arylimino)pyridines with *para*-Phenyl Substitution: Exploring Their Use as $N',N,N''$ -Supports in Iron Ethylene Polymerization Catalysis

Yizhou Wang <sup>1,2</sup>, Zheng Wang <sup>1,3</sup>, Qiuyue Zhang <sup>1</sup>, Yanping Ma <sup>1</sup>, Gregory A. Solan <sup>1,4,\*</sup>, Yang Sun <sup>1</sup>  
and Wen-Hua Sun <sup>1,2,\*</sup><sup>1</sup> Key Laboratory of Engineering Plastics, Beijing National Laboratory for Molecular Sciences, Institute of Chemistry Chinese Academy of Sciences, Beijing 100190, China<sup>2</sup> CAS Research/Education Center for Excellence in Molecular Sciences, University of Chinese Academy of Sciences, Beijing 100049, China<sup>3</sup> College of Science, Hebei Agricultural University, Baoding 071001, China<sup>4</sup> Department of Chemistry, University of Leicester, University Road, Leicester LE1 7RH, UK

\* Correspondence: gas8@leicester.ac.uk (G.A.S.); whsun@iccas.ac.cn (W.-H.S.); Tel.: +44-(0)116-2522096 (G.A.S.); +86-10-6255-7955 (W.-H.S.)

**Abstract:** Through the implementation of a one-pot strategy, five examples of non-symmetrical [ $N,N$ -diaryl-11-phenyl-1,2,3,7,8,9,10-heptahydrocyclohepta[ $b$ ]quinoline-4,6-diimine]iron(II) chloride complexes (aryl = 2,6-Me<sub>2</sub>Ph **Fe1**, 2,6-Et<sub>2</sub>Ph **Fe2**, 2,6-*i*-Pr<sub>2</sub>Ph **Fe3**, 2,4,6-Me<sub>3</sub>Ph **Fe4**, and 2,6-Et<sub>2</sub>-4-MePh **Fe5**), incorporating fused six- and seven-membered carbocyclic rings and appended with a remote *para*-phenyl group, were readily prepared. The molecular structures of **Fe2** and **Fe3** emphasize the variation in fused ring size and the skewed disposition of the *para*-phenyl group present in the  $N',N,N''$ -ligand support. Upon activation with MAO or MMAO, **Fe1–Fe5** all showed high catalytic activity for ethylene polymerization, with an exceptional level of  $35.92 \times 10^6$  g (PE) mol<sup>-1</sup> (Fe) h<sup>-1</sup> seen for mesityl-substituted **Fe4**/MMAO operating at 60 °C. All catalysts generated highly linear polyethylene with good control of the polymer molecular weight achievable via straightforward manipulation of run temperature. Typically, low molecular weight polymers with narrow dispersity ( $M_w/M_n = 1.5$ ) were produced at 80 °C (MMAO: 3.7 kg mol<sup>-1</sup> and MAO: 4.9 kg mol<sup>-1</sup>), while at temperatures between 40 °C and 50 °C, moderate molecular weight polymers were obtained (MMAO: 35.6–51.6 kg mol<sup>-1</sup> and MAO: 72.4–95.5 kg mol<sup>-1</sup>). Moreover, analysis of these polyethylenes by <sup>1</sup>H and <sup>13</sup>C NMR spectroscopy highlighted the role played by both  $\beta$ -H elimination and chain transfer to aluminum during chain termination, with the highest rate of  $\beta$ -H elimination seen at 60 °C for the MMAO-activated system and 70 °C for the MAO system.

**Keywords:** linear polyethylenes; high activity; molecular weight control; temperature effects; chain termination pathways



**Citation:** Wang, Y.; Wang, Z.; Zhang, Q.; Ma, Y.; Solan, G.A.; Sun, Y.; Sun, W.-H. Non-Symmetrically Fused Bis(arylimino)pyridines with *para*-Phenyl Substitution: Exploring Their Use as  $N',N,N''$ -Supports in Iron Ethylene Polymerization Catalysis. *Catalysts* **2024**, *14*, 213. <https://doi.org/10.3390/catal14030213>

Academic Editors: Alfonso Grassi and Marc Visseaux

Received: 4 February 2024

Revised: 9 March 2024

Accepted: 18 March 2024

Published: 21 March 2024



**Copyright:** © 2024 by the authors. Licensee MDPI, Basel, Switzerland. This article is an open access article distributed under the terms and conditions of the Creative Commons Attribution (CC BY) license (<https://creativecommons.org/licenses/by/4.0/>).

## 1. Introduction

Remarkable advances have been made in the design of iron and cobalt catalysts for olefin oligomerization and polymerization ever since the first disclosures in the late 1990s [1–4], which reflect the vital function played by the metal–ligand complex. With particular regard to the ligand,  $N,N,N$ -chelating 2,6-bis(arylimino)pyridines (**A**, Figure 1) have paved the way with a host of structural modifications reported over the last two and a half decades or so, culminating in notable effects on polymer structure and catalytic activity [5–11]. From an industrial perspective, 2-imino-1,10-phenanthroline complexes (**B**, Figure 1) have shown the greatest promise with a successful pilot-scale process for making linear  $\alpha$ -olefins using iron derivatives now being scaled up into a 200,000-ton process in China (in construction since November 2021) [12–14].

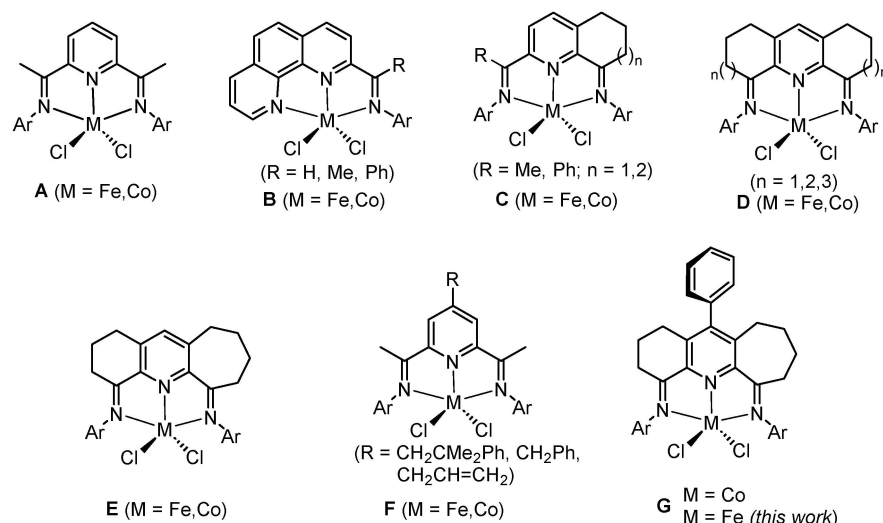


**Figure 1.** Bis(arylimino)pyridine iron(II)/cobalt(II) chlorides, **A**, and some key variations made to the *N,N,N*-ligand skeleton in **B–G**.

Elsewhere, the fusion of carbocyclic groups to the central pyridine in **A** has provided an effective means to not only enhance the thermostability and activity of the iron or cobalt catalyst [15–24] but also impart significant effects on the polymer products and catalytic activity. For example, cobalt-containing  $C_{n=1}$  (R = Me, Figure 1) incorporating a single six-membered fused ring [17] exhibited high activity for ethylene polymerization and, indeed, superior thermal stability to the prototypical cobalt catalyst **A** [1,2]. Similarly, iron and cobalt complexes containing a larger fused seven-membered ring,  $C_{n=2}$  (R = Ph, Figure 1) [18], showed improved thermal stability as well as a good catalytic lifetime. By contrast, doubly fused  $D_{2(n=1)}$ -type iron and cobalt complexes (Figure 1) [15], bearing two six-membered carbocyclic rings, have a tendency towards generating mixtures of oligomers and polyethylenes that limit their usefulness. However, this limitation can be overcome by increasing the ring size of the two fused rings, with the seven-membered ring-containing iron complex  $D_{2(n=2)}$  (Figure 1) [20], affording uniquely polyethylene. Furthermore, the bis(eight-membered) iron examples of  $D_{2(n=3)}$  (Figure 1) afford higher molecular weight polymer with very high activity (up to  $1.2 \times 10^7$  g (PE) mol<sup>-1</sup> (Fe) h<sup>-1</sup>) [17,22].

As a result of this fused ring strategy, bis(imino)pyridine complexes integrated with carbocyclic rings of different ring sizes have also started to emerge. For instance,  $E_{n=1/n=2}$ -type cobalt complexes (Figure 1) [23], containing both six- and seven-membered carbocycles, allow access to low molecular-weight vinyl-terminated polyethylenes ( $M_w$  range: 1.5–22.8 kg mol<sup>-1</sup>) with extremely narrow dispersity ( $M_w/M_n$  range: 1.5–2.1), materials that have received some attention as functional polymers for use in copolymerization [25–27]. In pursuit of better catalytic performance, iron examples of  $E_{n=1/n=2}$  have been shown to exhibit very high activity with levels reaching up to  $1.6 \times 10^7$  g (PE) mol<sup>-1</sup> (Fe) h<sup>-1</sup> at 40 °C forming bimodal polyethylenes [24].

As an alternative direction in *N,N,N* ligand design, the introduction of hydrocarbyl groups (e.g., CH<sub>2</sub>CH<sub>2</sub>Ph, CH<sub>2</sub>Ph, and CH<sub>2</sub>CH=CH<sub>2</sub>) to the *para*-position of the central pyridine in **A** has seen reports of iron and cobalt catalysts (**F**, Figure 1) that can influence molecular weight as well as the dispersity of the resulting polyethylene [28]. More recently, the introduction of a *para*-phenyl group to the central pyridine in cobalt-containing  $E_{n=1/n=2}$  to form **G** (Figure 1) has also seen unexpected enhancement effects on catalytic activity and molecular weight [29].

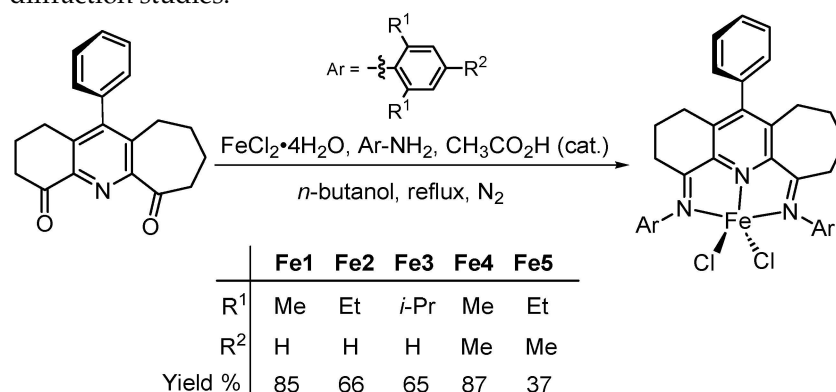
Given the superior catalytic performance generally seen for iron over cobalt in ethylene polymerization, we now target a series of *para*-phenyl-substituted ferrous examples of type **G** (Figure 1). In particular, five examples are disclosed that differ in the steric and electronic properties of the two *N*-aryl groups. To explore their use as catalysts in ethylene polymerization, a comprehensive evaluation has been undertaken that probes the type of

aluminum alkyl activator as well as the effect of run temperature, Al:Fe molar ratio, reaction time, and ethylene pressure. To shed some light on any effects imparted by the *para*-phenyl group in the polymerizations, comparisons are made throughout with structurally related doubly fused iron catalysts such as **D** and **E** (Figure 1). Besides this polymerization study, the synthetic details and characterization of all five iron(II) complexes are also presented.

## 2. Results and Discussion

### 2.1. Synthesis and Characterization of Fe1–Fe5

To access the [*N,N*-diaryl-11-phenyl-1,2,3,7,8,9,10-heptahydrocyclohepta[*b*]quinoline-4,6-diimine]iron(II) chloride complexes (aryl = 2,6-Me<sub>2</sub>Ph **Fe1**, 2,6-Et<sub>2</sub>Ph **Fe2**, 2,6-*i*-Pr<sub>2</sub>Ph **Fe3**, 2,4,6-Me<sub>3</sub>Ph **Fe4**, and 2,6-Et<sub>2</sub>-4-MePh **Fe5**), a straightforward one-pot approach proved effective. Specifically, by reacting 11-phenyl-1,2,3,7,8,9,10-heptahydrocyclohepta[*b*]quinoline-4,6-dione [24,29,30], the corresponding aniline and iron(II) chloride tetrahydrate in *n*-butanol at reflux under an atmosphere of nitrogen, in the presence of acetic acid as catalyst, **Fe1–Fe5** could be prepared as blue solids in yields of between 37% and 87% (Scheme 1). Attempts to make these complexes in a stepwise manner via the free ligand were hampered by difficulties in the purification of the diimine ligand due, in part, to the enamine tautomerism observed [15,24,31]. All five iron complexes proved stable when left to stand in the open air, but in solution, some evidence for oxidation could be detected. The characterization of these complexes was achieved using FT-IR spectroscopy, ESI mass spectrometry, and elemental analysis, while the crystals of **Fe2** and **Fe3** have been the subject of single X-ray diffraction studies.



**Scheme 1.** One-pot route to **Fe1–Fe5** from 11-phenyl-1,2,3,7,8,9,10-heptahydrocyclohepta[*b*]quinoline-4,6-dione.

Single crystals of **Fe2** and **Fe3** suitable for the X-ray determinations were grown in the glovebox under a nitrogen atmosphere by the slow diffusion of diethyl ether into a dichloromethane solution of the corresponding complex at ambient temperature. Perspective views of **Fe2** and **Fe3** are displayed in Figures 2 and 3; selected bond lengths and bond angles are presented in Table 1. For **Fe3**, the six- and seven-membered fused rings were disordered across both carbocyclic positions, an observation that has been noted previously [29]. Each structure consists of a single iron center coordinated by a tridentate *N,N*-diaryl-11-phenyl-1,2,3,7,8,9,10-heptahydrocyclohepta[*b*]quinoline-4,6-diimine ligand (aryl = 2,6-diethylphenyl **Fe2**, 2,6-diisopropylphenyl **Fe3**) and two chlorides to form a five-coordinate geometry, which can be best regarded as a distorted square pyramidal with Cl<sub>2</sub> occupying the apex and the three nitrogen atoms and Cl<sub>1</sub> the base. Some level of quantification of the degree of distortion can be demonstrated by using the tau value ( $\tau$ ), where  $\tau = 0$  represents an ideal square pyramidal and  $\tau = 1$  is an ideal trigonal bipyramid [32]. For **Fe2** and **Fe3**,  $\tau = 0.11$  and 0.21, respectively, which points towards modest distortions from an ideal square pyramidal, with the more sterically hindered 2,6-diisopropyl-containing **Fe3** causing a slightly larger distortion than in **Fe2**. The iron atom itself in each structure sits at a distance of 0.576 Å above the N1–N2–N3–Cl1 basal plane in **Fe2** and 0.536 Å in **Fe3**.

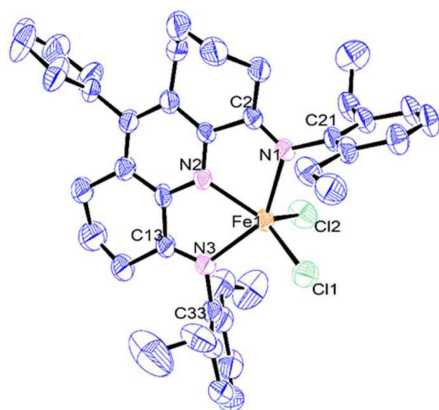


**Figure 2.** ORTEP representation of Fe2 with the thermal ellipsoids shown at the 50% probability level; all the hydrogen atoms and solvents have been omitted for clarity.

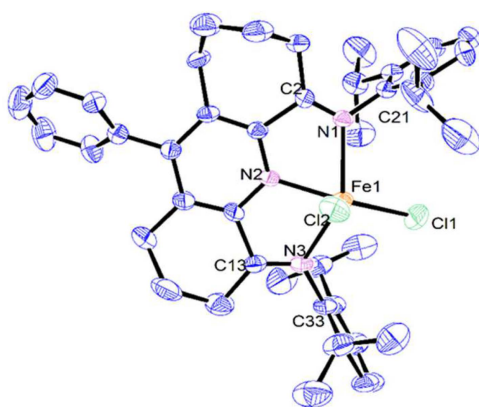


**Figure 3.** ORTEP representation of Fe3 with the thermal ellipsoids shown at the 50% probability level; all the hydrogen atoms have been omitted for clarity.

**Table 1.** Selected bond lengths and angles for Fe2 and Fe3.

	Fe2	Fe3
Bond lengths (Å)		
Fe(1)–N(2)	2.142(5)	2.076(3)
Fe(1)–N(1)	2.241(5)	2.228(2)
Fe(1)–N(3)	2.240(5)	2.169(3)
Fe(1)–Cl(1)	2.2824(18)	2.2537(10)
Fe(1)–Cl(2)	2.3023(19)	2.3177(9)
N(1)–C(2)	1.277(8)	1.208(15)
N(1)–C(21)	1.441(7)	1.443(4)
N(3)–C(13)	1.286(9)	1.281(15)
N(3)–C(33)	1.436(8)	1.447(4)
Bond angles (°)		
Cl(1)–Fe(1)–Cl(2)	107.94(9)	116.77(4)
N(2)–Fe(1)–Cl(1)	137.74(15)	152.59(9)
N(2)–Fe(1)–Cl(2)	114.30(15)	90.63(8)
N(1)–Fe(1)–Cl(1)	103.03(14)	98.63(7)
N(1)–Fe(1)–Cl(2)	98.74(15)	102.38(7)
N(3)–Fe(1)–Cl(1)	99.50(15)	100.58(8)
N(3)–Fe(1)–Cl(2)	99.99(16)	99.99(8)
N(3)–Fe(1)–N(1)	144.49(19)	139.70(11)
N(2)–Fe(1)–N(1)	72.52(18)	73.13(9)
N(2)–Fe(1)–N(3)	72.32(18)	73.54(10)

With regard to  $N',N,N''$ -Fe chelation, the Fe–N distance involving the central Fe– $N_{\text{pyridine}}$  bond is the shortest (Fe1–N2: 2.142(5) Å **Fe2**, 2.076(3) Å **Fe3**), as is typical of previous analogs and reflects the binding properties of the tridentate ligand [20,22,24]. For the longer exterior Fe– $N_{\text{imino}}$  bonds, some variation is evident between structure and those in **Fe2** comparable (2.241(5) and 2.240(5) Å), while in **Fe3** the Fe1–N1 distance (2.228(2) Å) is noticeably longer than the Fe1–N3 one (2.169(3) Å), likely reflecting the steric properties of the larger 7-membered carbocycle and the bulky *ortho*-isopropyl groups. Notably, in the non-phenyl substituted iron(II) counterpart of **Fe3**, **E** (M = Fe, Ar = diisopropylphenyl, Figure 1), the exterior Fe– $N_{\text{imine}}$  distances are equivalent (2.216(1) Å) [24], which suggests the *para*-phenyl group in **Fe3** exerts some long-range influence on the binding properties of this particular  $N',N,N''$ -ligand. On the other hand, a similar comparison of the Fe– $N_{\text{pyridine}}$  bond distance in **Fe3** with that in **E** (M = Fe, Ar = diisopropylphenyl, Figure 1) shows only a modest lengthening in the former (2.076(3) vs. 2.060(1) Å). For both **Fe2** and **Fe3**, some deviation from coplanarity between the exterior imine groups and pyridine ring is seen, as is evidenced by the N2–C1–C2–N1 torsion angles (11.82° **Fe2**, 11.40° **Fe3**) and N2–C14–C13–N3 (8.12° **Fe2**, 10.90° **Fe3**), which can be credited to the strain imparted by the carbocyclic groups on the  $N',N,N''$ -ligand framework.

As is common to many bis(arylimino)pyridine-iron complexes, the two *N*-aryl groups are inclined essentially perpendicularly to the  $N',N,N''$ -coordination plane in both **Fe2** and **Fe3**, thereby positioning the *ortho*-substituents above and below this plane. The six- and seven-membered carbocycles in the chelating ligand adopt puckered arrangements, with the latter showing the most flexibility. The *para*-phenyl groups themselves in **Fe2** and **Fe3** adopt skewed dispositions with respect to the neighboring pyridine plane (tors. C9–C8–C15–C20 84.66° **Fe2**, 56.16° **Fe3**) due to the rotary flexibility of the *para*-phenyl group; similar flexibility has been noted in their cobalt analogs [29]. There are no intermolecular contacts of note.

In the FT-IR spectra of **Fe1–Fe5** (Figures S14–S18), characteristic peaks were identifiable for the imine double bonds between 1604 and 1617  $\text{cm}^{-1}$ , a range that is quite typical for coordinated imine groups in related iron(II) complexes [20,22,24,33,34]. In addition, the micro-analytical data for each iron complex lend good support for compositions of the type  $\text{LFeCl}_2$ .

## 2.2. Ethylene Polymerization Investigations Using **Fe1–Fe5**

As has been noted previously, methylaluminumoxane (MAO) and modified methylaluminumoxane (MMAO) are among the most effective activators for iron-based ethylene polymerization catalysis [20,22,24]. Accordingly, these two aluminumoxanes were taken forward as part of parallel studies with the purpose of exploring not only structure–activity/polymer correlations in **Fe1–Fe5** but also the impact of the type of activator on these correlations. All polymerizations were conducted in toluene, with the ethylene pressure initially set at 10 atm.

### 2.2.1. Polymerization Studies Using **Fe1–Fe5** under Activation with MMAO

To allow a workable set of polymerization conditions using MMAO, **Fe4** was initially employed as the test precatalyst, and the most effective conditions identified were then extended to evaluate **Fe1–Fe3** and **Fe5**; the complete set of results is shown in Table 2.

To examine the effect of run temperature, the polymerizations using **Fe4**/MMAO were initially carried out at temperatures between 40 °C and 80 °C with the Al:Fe molar ratio fixed at 2500:1 (**Fe4**: 1  $\mu\text{mol}$ ) and a run time of 30 min (entries 1–5, Table 2). Inspection of the results reveals the catalytic activity reached a maximum of  $19.14 \times 10^6 \text{ g (PE) mol}^{-1} (\text{Fe}) \text{ h}^{-1}$  at 60 °C and still remained high with the temperature at 80 °C, with a level of  $7.32 \times 10^6 \text{ g (PE) mol}^{-1} (\text{Fe}) \text{ h}^{-1}$  noted (Figure 4). These performance characteristics reflect the appreciable thermal stability of **Fe4**. With regard to the polymer generated, the GPC traces indicate that the molecular weight rapidly decreased from 51.6  $\text{kg mol}^{-1}$  to 3.7  $\text{kg mol}^{-1}$  as the temperature was increased from 40 °C to 80 °C, respectively, in line with the higher rate of chain termination at higher temperatures [24]. Furthermore, the dispersity of the polymer generated significantly narrowed as the temperature was increased ( $M_w/M_n$ : from 14.2 to 1.5), with an initially

bimodal distribution becoming unimodal at temperatures in excess of 60 °C. This evidence of bimodality at lower temperatures could be attributed to the different chain transfer pathways operational, namely  $\beta$ -H elimination and chain transfer to aluminum alkyl species (e.g.,  $\text{AlMe}_3$ ) in MMAO [4,10,24]. Alternatively, the bimodality could be caused by the presence of oxidized iron complexes, leading to additional active centers [22]. On the other hand, at higher run temperatures, it would seem plausible that either a single active center predominates or a single chain transfer pathway becomes prevalent [22].

**Table 2.** Ethylene polymerization screening using Fe1–Fe5 with MMAO as activator <sup>a</sup>.

Entry	Precat.	Al:Fe	T (°C)	t (min)	Mass of PE (g)	Activity <sup>b</sup>	$M_w^c$	$M_w/M_n^c$	$T_m$ (°C) <sup>d</sup>
1	Fe4	2500	40	30	5.14	10.28	51.6	14.2	131.1
2	Fe4	2500	50	30	8.69	17.38	35.6	10.7	129.8
3	Fe4	2500	60	30	9.57	19.14	9.8	3.1	130.0
4	Fe4	2500	70	30	8.91	17.82	4.8	1.5	127.7
5	Fe4	2500	80	30	3.66	7.32	3.7	1.5	128.8
6	Fe4	1500	60	30	2.57	5.14	46.0	2.8	132.4
7	Fe4	1750	60	30	9.75	19.50	36.2	2.7	133.1
8	Fe4	2000	60	30	17.05	34.10	81.3	9.6	131.8
9	Fe4	2250	60	30	12.50	25.00	85.1	7.0	132.8
10	Fe4	2000	60	5	8.12	97.44	13.7	3.5	128.8
11	Fe4	2000	60	15	11.27	45.08	23.0	3.9	131.2
12	Fe4	2000	60	45	18.01	24.01	90.6	9.1	135.3
13	Fe4	2000	60	60	18.24	18.24	94.3	9.2	132.6
14 <sup>e</sup>	Fe4	2000	60	30	0.61	1.22	0.8	1.3	120.2
15 <sup>f</sup>	Fe4	2000	60	30	8.98	17.96	79.0	7.4	132.0
16	Fe1	2000	60	30	12.89	25.78	26.4	6.4	129.5
17	Fe2	2000	60	30	14.67	29.34	70.0	6.9	131.9
18	Fe3	2000	60	30	5.33	10.66	51.6	8.1	131.1
19	Fe5	2000	60	30	3.82	7.64	69.4	13.6	130.1

<sup>a</sup> Conditions: MMAO as an activator, 1.0  $\mu\text{mol}$  of the iron precatalyst, 100 mL of toluene, and 10 atm of ethylene;

<sup>b</sup> Values in units of  $10^6 \text{ g (PE) mol}^{-1} (\text{Fe}) \text{ h}^{-1}$ ; <sup>c</sup>  $M_w$  and  $M_n$  in units of  $\text{kg mol}^{-1}$ , determined by GPC; <sup>d</sup> Determined by DSC; <sup>e</sup> 1 atm of ethylene; <sup>f</sup> 5 atm of ethylene.

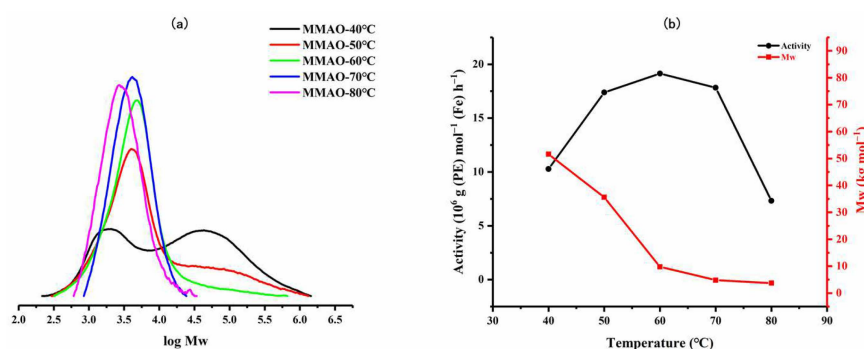


**Figure 4.** (a) GPC traces of the polyethylenes generated using Fe4/MMAO at different temperatures and (b) plots of catalytic activity and polymer molecular weight as a function of run temperature.

Thereafter, the polymerizations using Fe4/MMAO were undertaken at Al:Fe molar ratios between 1500:1 and 2500:1, with the temperature kept at 60 °C (entries 3 and 6–9, Table 2). As can be seen from the tabulated results, the highest activity of  $34.10 \times 10^6 \text{ g (PE) mol}^{-1} (\text{Fe}) \text{ h}^{-1}$  was recorded with the ratio at 2000:1, which was extremely high when compared with previously reported  $N,N,N$ -iron catalysts under comparable reaction conditions [20,22,24]. With the Al:Fe molar ratio gradually increasing from 1500:1 to 2500:1, the highest molecular weight polymer of  $85.1 \text{ kg mol}^{-1}$  was recorded at 2250:1, while the lowest of  $9.8 \text{ kg mol}^{-1}$  was obtained at 2500:1 (Figure 5). This dramatic decline in molecular weight with ratios exceeding 2250:1 reflects the critical value of aluminoxane necessary for chain transfer from the active species to aluminum in MMAO becomes significant [22,24].

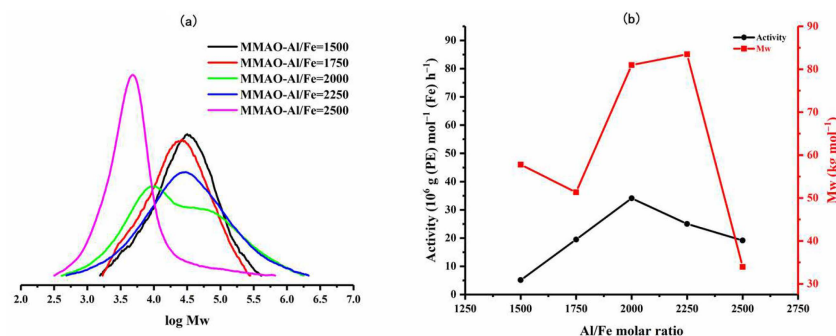


**Figure 5.** (a) GPC traces of the polyethylenes generated using **Fe4**/MMAO at various Al:Fe molar ratios and (b) plots of catalytic activity and polymer molecular weight as a function of Al:Fe molar ratio.

To explore the effect of the run time using **Fe4**/MMAO, five separate polymerizations were conducted over 5, 15, 30, 45, and 60 min with the Al:Fe molar ratio kept at 2000:1 and the temperature at 60 °C (entries 8 and 10–13, Table 2). As time elapsed, the activity rapidly decreased from  $97.44 \times 10^6$  g (PE) mol<sup>-1</sup> (Fe) h<sup>-1</sup> after 5 min to  $18.24 \times 10^6$  g (PE) mol<sup>-1</sup> (Fe) h<sup>-1</sup> by the one-hour mark (Figure 6), suggesting a short induction period for this catalyst and a relatively long lifetime for the active species [20,22,24]. With respect to the molecular weight data, a gradual increase was observed in the first 15 min, followed by a rapid increase between 15 and 30 min, and then assuming a more constant level of molecular weight as the run reached 60 min. In terms of the dispersity, a steady increase was noted over the first 15 min ( $M_w/M_n$ : from 3.5 to 3.9) before a significant broadening and the onset of some bimodality were seen between 30 and 60 min ( $M_w/M_n$ : from 9.1 to 9.6), suggesting the formation of another active species [22] or an additional chain transfer pathway becoming operative.

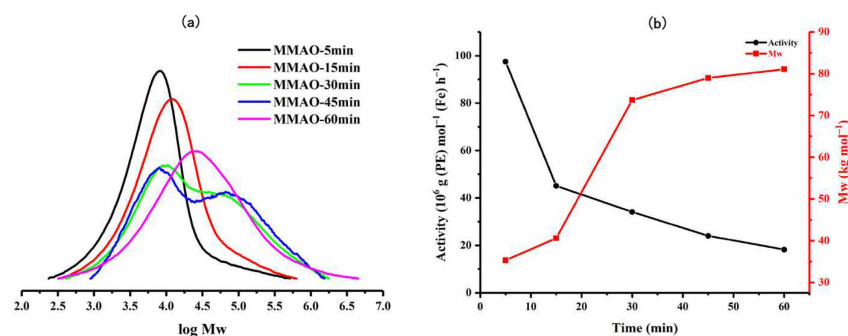


**Figure 6.** (a) GPC traces of the polyethylenes generated using **Fe4**/MMAO as the run time was varied, and (b) plots of catalytic activity and polymer molecular weight as a function of reaction time.

To investigate the effect of the ethylene pressure on the polymerizations using **Fe4**/MMAO, the runs were additionally conducted at pressures of 1 and 5 atm with the Al:Fe molar ratio fixed at 2000:1 and the temperature kept at 60 °C (entries 8, 14, and 15, Table 2). At 1 atm, the lowest activity of  $1.22 \times 10^6$  g (PE) mol<sup>-1</sup> (Fe) h<sup>-1</sup> was observed, which can be credited to the relatively low solubility of ethylene in toluene at this pressure [24]. On the other hand, at 10 atm, the activity attained its highest value ( $34.10 \times 10^6$  g (PE) mol<sup>-1</sup> (Fe) h<sup>-1</sup>) and indeed was around twice that seen at 5 atm ( $17.96 \times 10^6$  g (PE) mol<sup>-1</sup> (Fe) h<sup>-1</sup>), underscoring the beneficial effect of ethylene pressure on productivity.

On the strength of the most effective set of conditions identified using **Fe4**/MMAO (run temperature = 60 °C, Al:Fe = 2000:1, run time = 30 min,  $P_{C_2H_4}$  = 10 atm), the remaining iron precatalysts, **Fe1**, **Fe2**, **Fe3**, and **Fe5**, were then studied accordingly (entries 16–19, Table 2). All catalysts displayed high activity (range:  $7.64$ – $34.10 \times 10^6$  g (PE) mol<sup>-1</sup> (Fe) h<sup>-1</sup>), with the relative order being: **Fe4** (2,4,6-trimethyl) > **Fe2** (2,6-diethyl) > **Fe1** (2,6-dimethyl) > **Fe3** (2,6-diisopropyl) > **Fe5** (2,6-diethyl-4-methyl) (Figure 7). These results suggest that less

bulky *ortho*-R<sup>1</sup> groups are, in general, beneficial to the process of ethylene coordination/migratory insertion [24,30,35]. Nevertheless, it is evident that there are some anomalies in this structure/activity correlation, which could be attributable to the long-range effect of the *para*-phenyl group on carbocyclic ring flexibility and, in turn, *N*-aryl group binding/inclination [29].

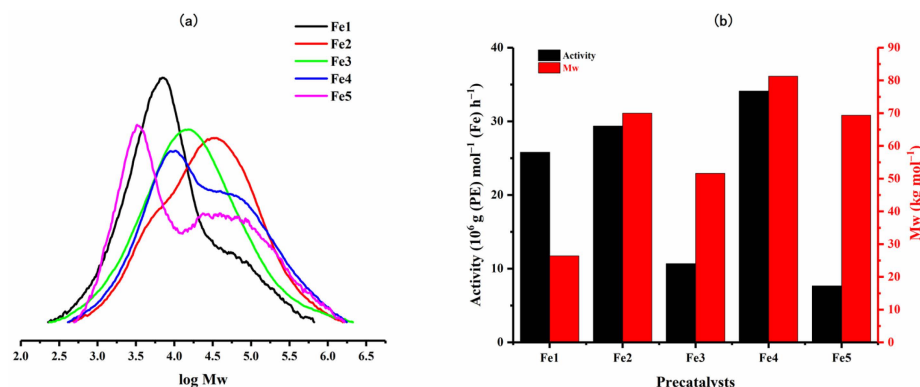


**Figure 7.** (a) GPC traces of the polyethylenes generated using **Fe1–Fe5** with MMAO as an activator and (b) a bar chart showing catalytic activity and polymer molecular weight with respect to the iron precatalyst employed.

As for the GPC traces, moderate molecular weight polymer ( $M_w$ : 26.4–81.3  $\text{kg mol}^{-1}$ ) was obtained for all precatalysts, while the dispersities were in all cases broad ( $M_w/M_n$ : 6.4–13.6). Indeed, the least hindered **Fe4**-formed polymer exhibited a higher molecular weight than that seen for diisopropyl-containing **Fe3**, which was quite different from previous studies where larger *ortho*-substituents tend to promote higher molecular weight material [20,22,24]. The reason for this observation remains uncertain but may conceivably be attributed to the *para*-phenyl group somehow influencing chain propagation, which is most apparent in the more sterically hindered **Fe3**. By contrast, the less bulky **Fe1** (2,6-dimethyl) and **Fe2** (2,6-diethyl) are less affected by the *para*-phenyl group, resulting in the molecular weight of the polymer formed by **Fe2** being greater than that of **Fe1**, an observation that can be credited to the bulkier *ortho*-ethyl groups better protecting the active center [20,22,24].

To understand the performance characteristics of the current catalysts in terms of activity and polymer molecular weight and dispersity, data for mesityl-containing **Fe4** (denoted in **G** as in Figure 1) are collected in Figure 8 alongside that for some previously reported iron systems incorporating doubly fused carbocycles. From this bar chart, it is evident that the highest activity of these iron complexes follows the order: **G** (**Fe4**: this work)  $\gg E_{n=1/n=2} > D_{2(n=3)} \approx D_{2(n=2)}$  (Figure 1) [20,22,24]. Evidently, the *para*-phenyl group in **G** exerts a positive effect on catalytic activity, which is most striking when compared to its non-phenyl substituted comparator  $E_{n=1/n=2}$ , a finding that mirrors that seen with the cobalt counterparts [29]. While the origin of the effect remains uncertain, we consider the *para*-phenyl group to have a limited effect on the binding properties of this mesityl-substituted  $N',N,N''$ -ligand. Indeed, analysis of the X-ray structure of the 2,6-diethylphenyl-containing **Fe2** showed no evidence of uneven binding of the chelating ligand, a feature that was notably apparent in the bulkier derivative **Fe3** (see above). One plausible explanation for **G** (**Fe4**) being more active than  $E_{n=1/n=2}$  stems from the electron-withdrawing properties of the phenyl group and the impact this has on the ethylene coordination and insertion at the active iron center. Furthermore, the molecular weight of the polyethylene decreases in the following order:  $D_{2(n=3)} > \mathbf{G} (\mathbf{Fe4}: \text{this work}) > E_{n=1/n=2} > D_{2(n=2)}$ . This finding shows that the presence of both the large eight-membered fused structure ( $D_{2(n=3)}$ ) and the *para*-phenyl group in **G** (**Fe4**) can have a favorable effect on the molecular weight of the polymer, observations that are similar to those observed for their cobalt analogs. In short, the introduction of the *para*-phenyl group to the  $N',N,N''$ -ligand periphery in **G** has

the effect of promoting the catalytic activity and increasing the molecular weight of the polymer for both iron and cobalt complexes. In terms of the optimal run temperature, **G (Fe4: this work)** proved the most effective by operating effectively at 60 °C, which compares to 40 °C for the non-*para*-phenyl substituted analog  $E_{n=1/n=2}$  [24], a result that suggests the *para*-phenyl group can also help provide a more stable active species at higher operating temperatures. As a final point, it can be seen from the figure that the dispersity is broad for all of these iron complexes, in line with the different chain transfer pathways that are operational.

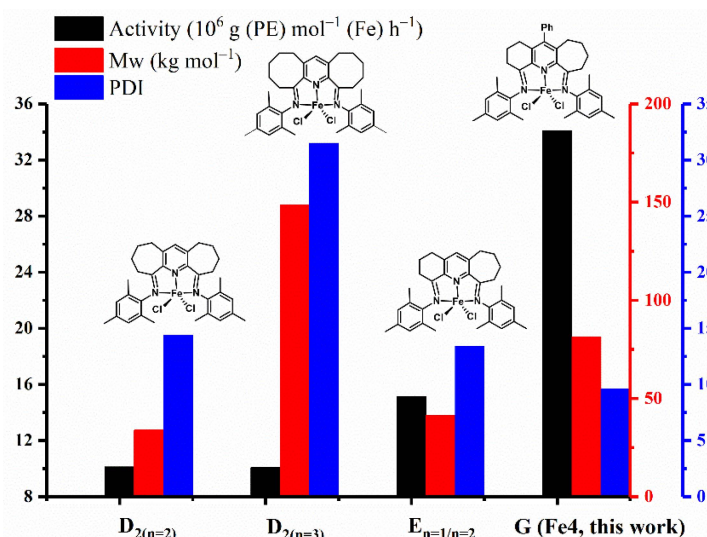


**Figure 8.** Comparison of the catalytic activity, polymer molecular weight, and dispersity obtained using **G (Fe4, this work)** with that for carbocyclic-fused iron pre-catalysts,  $D_{2(n=2)}$ ,  $D_{2(n=3)}$ , and  $E_{n=1/n=2}$ ; all polymerizations were conducted using MMAO at 10 atm of ethylene and under optimal reaction conditions.

### 2.2.2. Polymerization Studies Using Fe1–Fe5 under Activation with MAO

To enable a comparison with the polymerization runs performed with MMAO, MAO was also employed in the activation of **Fe1–Fe5**. As before, **Fe4** was initially employed as the test pre-catalyst so as to identify an effective set of reaction conditions that could be used to screen the other iron pre-catalysts (Table 3).

In the first instance, the polymerization runs were performed using **Fe4**/MAO at run temperatures of between 40 and 80 °C (entries 1–5, Table 3) with the Al:Fe molar ratio fixed at 2500:1 and the run time at 30 min (entries 1–5, Table 3). The highest catalytic activity of  $30.58 \times 10^6 \text{ g (PE) mol}^{-1} (\text{Fe}) \text{ h}^{-1}$  was achieved at 60 °C, reflecting the outstanding thermal stability of this iron catalyst. Moreover, the molecular weight of the polymer dropped rapidly from  $95.5 \text{ kg mol}^{-1}$  at 40 °C to  $4.9 \text{ kg mol}^{-1}$  at 80 °C (Figure S1), which can be attributed to the higher rate of chain transfer at high temperatures [24]. As for the polymer dispersity, this decreased from 18.5 (40 °C) to 1.5 (80 °C) as the temperature increased, which manifests itself in the initially bimodal distribution becoming unimodal, findings that likely stem from the two chain transfer pathways becoming less competitive at higher temperatures [9,10,36].

Following this, the polymerizations were evaluated with Al:Fe molar ratios of 1000:1, 1500:1, 2000:1, 2500:1, and 3000:1 with the temperature fixed at 60 °C (entries 3 and 6–9, Table 3). As a result, the highest activity of  $35.92 \times 10^6 \text{ g (PE) mol}^{-1} (\text{Fe}) \text{ h}^{-1}$  was noted with the ratio of 2000:1 (Figure S2), which was marginally higher than the optimal activity for the MMAO runs ( $34.10 \times 10^6 \text{ g (PE) mol}^{-1} (\text{Fe}) \text{ h}^{-1}$ ). As for the molecular weight of the polymer, this was found to markedly decrease from 161.2 to  $32.3 \text{ kg mol}^{-1}$  as the Al:Fe molar ratio was increased, in line with a higher rate of chain transfer [24].

To shed light on the catalytic lifetime of the active center in **Fe4**/MAO, the polymerizations were carried out at different run times with the temperature and Al:Fe molar ratio kept at 60 °C and 2000:1, respectively. As expected, an exceptionally high activity of

$84.96 \times 10^6$  g (PE) mol<sup>-1</sup> (Fe) h<sup>-1</sup> was observed after 5 min (entry 10, Table 3), which then progressively decreased to  $18.65 \times 10^6$  g (PE) mol<sup>-1</sup> (Fe) h<sup>-1</sup> at 60 min (entry 13, Table 3), suggesting a short induction period and an excellent lifetime for the active center [20]. Meanwhile, the molecular weight of the polyethylene increased from 16.8 to 168.0 kg mol<sup>-1</sup> over time (Figure S3), while the dispersity ( $M_w/M_n$ ) increased from 3.8 to 16.6 in a similar manner to that seen for Fe4/MMAO.

**Table 3.** Ethylene polymerization screening using Fe1–Fe5 with MAO as activator <sup>a</sup>.

Entry	Precat.	Al:Fe	T (°C)	t (min)	Mass of PE (g)	Activity <sup>b</sup>	$M_w^c$	$M_w/M_n^c$	$T_m$ (°C) <sup>d</sup>
1	Fe4	2500	40	30	6.04	12.08	95.5	18.5	130.2
2	Fe4	2500	50	30	10.03	20.06	72.4	11.7	130.7
3	Fe4	2500	60	30	15.29	30.58	65.0	8.8	131.7
4	Fe4	2500	70	30	9.85	19.70	18.4	3.0	130.3
5	Fe4	2500	80	30	5.05	10.10	4.9	1.5	132.7
6	Fe4	1000	60	30	10.54	21.08	161.2	8.4	132.1
7	Fe4	1500	60	30	12.52	25.04	152.5	13.8	132.3
8	Fe4	2000	60	30	17.96	35.92	129.0	11.4	132.3
9	Fe4	3000	60	30	14.80	29.60	32.3	4.3	130.7
10	Fe4	2000	60	5	7.08	84.96	16.8	3.8	129.4
11	Fe4	2000	60	15	11.05	44.20	29.7	6.1	130.0
12	Fe4	2000	60	45	18.13	24.17	142.1	15.4	131.5
13	Fe4	2000	60	60	18.65	18.65	168.0	16.6	133.0
14 <sup>e</sup>	Fe4	2000	60	30	0.84	1.68	3.4	4.0	124.8
15 <sup>f</sup>	Fe4	2000	60	30	7.04	14.08	130.7	13.0	132.7
16	Fe1	2000	60	30	14.10	28.20	48.9	8.8	131.1
17	Fe2	2000	60	30	10.18	20.36	59.2	8.5	131.4
18	Fe3	2000	60	30	6.52	13.04	35.2	7.0	131.4
19	Fe5	2000	60	30	8.73	17.46	50.2	8.8	132.2

<sup>a</sup> Conditions: MAO as an activator, 1.0 μmol of the iron precatalyst, 100 mL of toluene, 10 atm of ethylene; <sup>b</sup> Values in units of  $10^6$  g (PE) mol<sup>-1</sup> (Fe) h<sup>-1</sup>; <sup>c</sup>  $M_w$  and  $M_n$  in units of kg mol<sup>-1</sup>, determined by GPC; <sup>d</sup> Determined by DSC; <sup>e</sup> 1 atm of ethylene; <sup>f</sup> 5 atm of ethylene.

On lowering the ethylene pressure from 10 atm to 1 atm using Fe4/MAO, a sharp decline in activity was observed from  $35.92 \times 10^6$  g (PE) mol<sup>-1</sup> (Fe) h<sup>-1</sup> to  $0.84 \times 10^6$  g (PE) mol<sup>-1</sup> (Fe) h<sup>-1</sup> (entries 8, 14, and 15, Table 3), which most likely derives from the lower solubility of ethylene in toluene at lower pressure [23,29]. Furthermore, the molecular weight of the polyethylene decreased noticeably from 129.0 to 3.4 kg mol<sup>-1</sup> by dropping the pressure from 10 atm to 1 atm, an observation that supports the lower rates of chain propagation that are operational at lower pressure [24]. In addition, the molecular weight of the polyethylene formed during the Fe4/MAO runs was higher than that seen using Fe4/MMAO, reflecting the lower rate of chain transfer with MAO.

To gain further insight into the role of the *N*-aryl variations in Fe1–Fe5, the optimal conditions identified using Fe4/MAO (namely reaction temperature of 60 °C, Al:Fe molar ratio of 2000:1, ethylene pressure of 10 atm, and run time of 30 min) were deployed to evaluate the other iron precatalysts, Fe1–Fe3 and Fe5 (entries 16–19, Table 3). All iron complexes exhibited high activity (range:  $13.04$ – $35.92 \times 10^6$  g (PE) mol<sup>-1</sup> (Fe) h<sup>-1</sup>) and produced highly linear polyethylenes ( $T_m$ : 131–133 °C) with broad dispersities. On analysis of their relative performance, the catalytic activity decreased in the following order: Fe4 (aryl = 2,4,6-trimethylphenyl) > Fe1 (aryl = 2,6-dimethylphenyl) > Fe2 (aryl = 2,6-diethylphenyl) > Fe5 (aryl = 2,6-diethyl-4-methylphenyl) > Fe3 (aryl = 2,6-diisopropylphenyl) (Figure S4). As is evident, the precatalysts bearing the least bulky substituents in the *ortho* positions of the *N*-aryl groups, Fe4 and Fe1, exhibited higher activity due to the faster rates of ethylene insertion and chain propagation [24,30,35]. Moreover, mesityl-containing Fe4 produced the highest molecular weight polyethylene of the series, which was also seen for the MMAO runs, but nonetheless unexpected when compared with previous work in which the most sterically hindered complex

usually affords the highest molecular weight polymer. This unusual finding plausibly arose from the very high activity seen for **Fe4**, thereby inhibiting chain transfer.

### 2.3. Structural Analysis of the Polyethylene

The microstructural characteristics of polymers are of great significance to their mechanical properties and, in turn, their processing ability. As has already been highlighted, the DSC thermograms for the polyethylenes produced in this work typically display  $T_m$  values of  $>130$  °C in accordance with highly linear polymers (see Tables 2 and 3) [16,18,20,23,24]. To obtain more information, selected polyethylene samples were further analyzed by  $^1\text{H}$  and  $^{13}\text{C}$  NMR spectroscopy with a view to understanding how run temperature and the type of aluminum activator impact the microstructure.

To begin with, we looked at the polymers generated using **Fe4**/MMAO at run temperatures of 40, 50, 60, 70, and 80 °C, where variations in molecular weight and dispersity were observed. To engender suitable solubility, these polymer samples were dissolved in the 1,1,2,2-tetrachloroethane- $d_2$  at 100 °C, and their  $^1\text{H}$  NMR spectra were recorded at a similar temperature (entries 1–5, Table 2). For the  $^1\text{H}$  NMR spectrum of the polyethylene obtained using **Fe4**/MMAO at 80 °C (entry 5, Table 2:  $M_w = 3.7$  kg mol $^{-1}$ ,  $M_w/M_n = 1.5$ ), a high-intensity resonance at  $\delta$  1.32 ppm for the  $-(\text{CH}_2)_n-$  repeat unit confirms the strictly linear nature of the polyethylene (Figure 9). Either side of this signal shows lower intensity peaks, which correspond to an  $n$ -propyl group ( $\text{H}_f$ ,  $\text{H}_e$ , and  $\text{H}_d$ ), while the more downfield region reveals multiplet peaks at  $\delta$  5.00 and 5.85 ppm, which can be assigned to a vinyl end-group ( $\text{H}_a$  and  $\text{H}_b$ ). Evidently, the latter observation highlights the involvement of  $\beta$ -H elimination to metal or monomer during chain termination [24]. Moreover, by considering the integral ratio of vinyl  $\text{H}_b$  to methyl chain-end  $\text{H}_f$  (1/18.82) [29,37,38], the molar ratio of the unsaturated polymer chain to the saturated polymer chain can be determined as 0.379 (see SI), a value that implies the additional presence of a fully saturated polymer in line with chain transfer to aluminum being also operational [4,5]. Further support for these assignments was provided by the  $^{13}\text{C}$  NMR spectrum, which reveals a high-intensity peak around  $\delta$  29.43 ppm, which corresponds to the  $-(\text{CH}_2)_n-$  repeat unit, along with lower intensity peaks at  $\delta$  13.72, 22.38, and 31.66 ppm for an  $n$ -propyl end-group and weaker downfield peaks at  $\delta$  113.85 and 138.78 ppm for a terminal vinyl group (Figure 10) [24]. The absence of resonances corresponding to an isobutyl end-group rules out any chain transfer to aluminum-isobutyl species present within MMAO [30], which suggests that chain transfer to aluminum occurs solely with aluminum-methyl species.

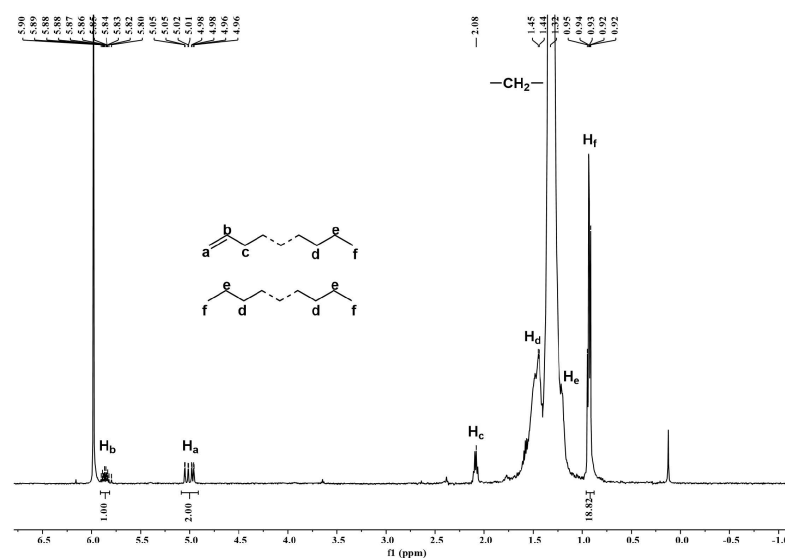


**Figure 9.**  $^1\text{H}$  NMR spectrum of the polyethylene produced using **Fe4**/MMAO operating at 80 °C (entry 5, Table 2); recorded at 100 °C in 1,1,2,2-tetrachloroethane- $d_2$ .

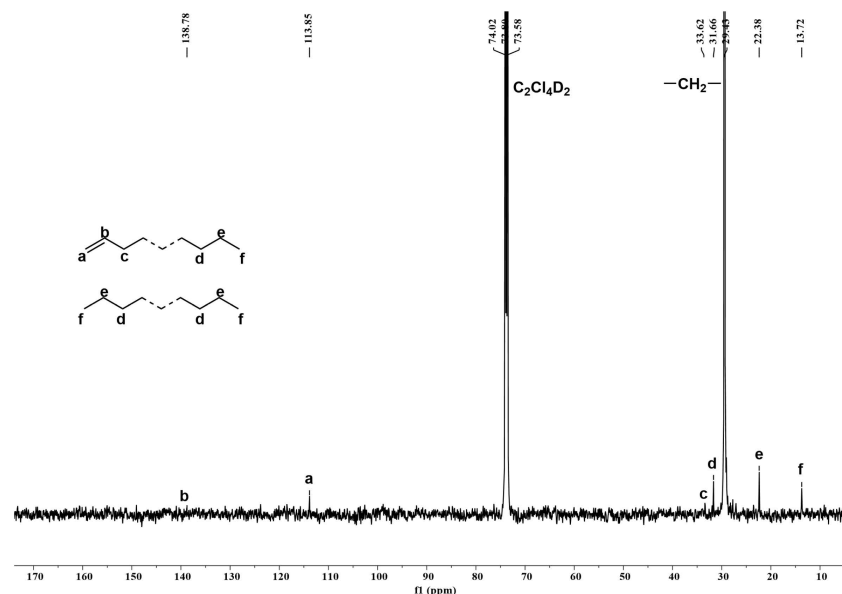


**Figure 10.**  $^{13}\text{C}$  NMR spectrum of the polyethylene produced using **Fe4**/MMAO operating at  $80\text{ }^\circ\text{C}$  (entry 5, Table 2); recorded at  $100\text{ }^\circ\text{C}$  in 1,1,2,2-tetrachloroethane- $d_2$ .

The  $^1\text{H}$  NMR spectra for the polymers produced using **Fe4**/MMAO at the lower run temperatures ( $40\text{--}70\text{ }^\circ\text{C}$ , entries 1–4, Table 2) revealed similar features, with signals characteristic of the  $-(\text{CH}_2)_n-$  repeat unit and weaker peaks for the  $n$ -propyl and vinyl chain-ends (Figures S5–S8). However, the molar ratio of unsaturated to saturated polymer chains showed some notable variations, with the value reaching a maximum of 1.98 at  $60\text{ }^\circ\text{C}$  (Figure 11), which implies that  $\beta$ -H elimination assumes the main chain termination pathway at this point. However, at temperatures below  $60\text{ }^\circ\text{C}$ , the ratio drops to 0.394 ( $50\text{ }^\circ\text{C}$ ) and then 0.108 ( $40\text{ }^\circ\text{C}$ ), reflecting the importance of chain transfer to aluminum-methyl species in MMAO at these temperatures. Evidently, the chain transfer pathways are affected by the run temperature, with the highest rate of  $\beta$ -H elimination occurring at  $60\text{ }^\circ\text{C}$ , which also corresponds to the optimal temperature in terms of catalytic activity.

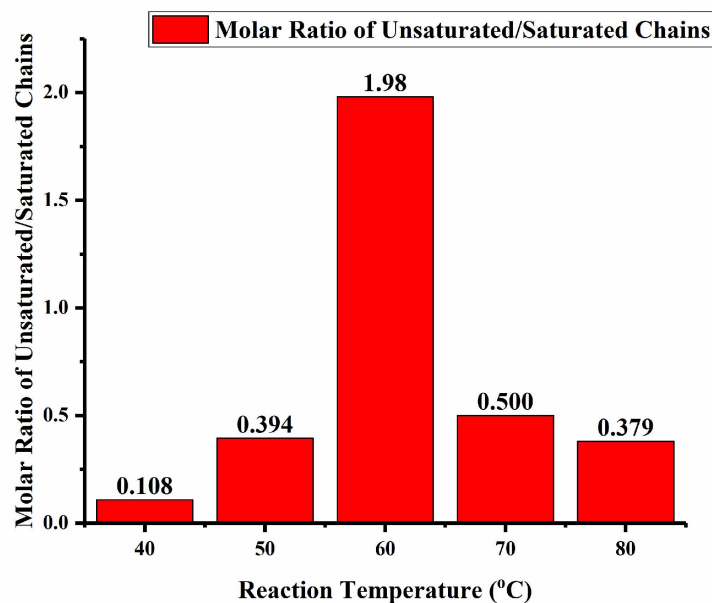


**Figure 11.** Bar chart showing the ratio of unsaturated to saturated chains for the polymer obtained as a function of run temperature using **Fe4**/MMAO as catalyst (entries 1–5, Table 2).

To appreciate the effect of the aluminum activator on these chain transfer pathways, the polyethylenes produced using Fe4/MAO over the same run temperature range (40–80 °C) as that used for Fe4/MMAO were similarly investigated by  $^1\text{H}$  NMR spectroscopy. Once again, the  $^1\text{H}$  NMR spectra of all five polymer samples revealed peaks characteristic of a highly linear polymer backbone along with varying amounts of chain end vinyl and *n*-propyl groups (Figures S9–S13). Interestingly, the highest rate of  $\beta$ -H elimination using Fe4/MAO was found at 70 °C (Figure 12), as evidenced by the highest molar ratio of unsaturated to saturated polymer chains in the polymer (1.05:  $\text{H}_b:\text{H}_f = 1/8.71$ ). Nevertheless, this value was lower than that seen with the MMAO-activated system, an observation that reflects the differences in the type of aluminoxane and their impact on the competing chain transfer pathways.

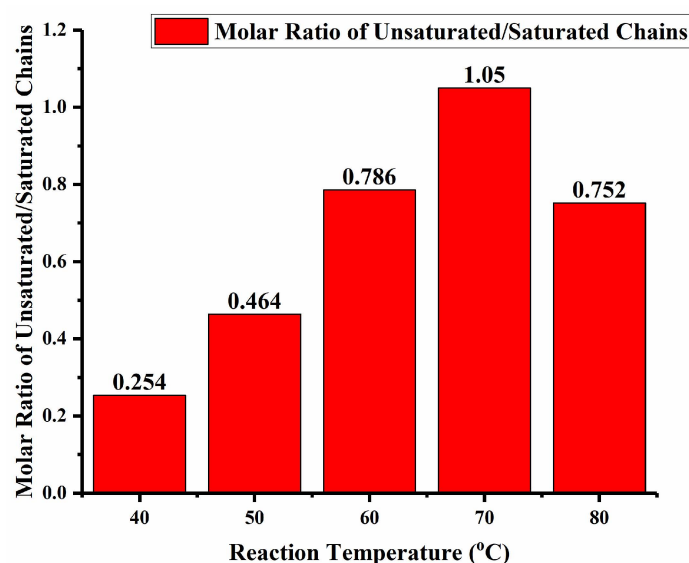


**Figure 12.** Bar chart showing the ratio of unsaturated to saturated chains for the polymer obtained as a function of run temperature using Fe4/MAO as catalyst (entries 1–5, Table 3).

### 3. Materials and Methods

#### 3.1. General Considerations

All operations making use of moisture and/or air-sensitive compounds were conducted under a nitrogen atmosphere by using standard Schlenk techniques or in a nitrogen-filled glovebox. Toluene, the solvent used for the polymerization studies, was heated to reflux for more than 12 h over sodium benzophenone and distilled under nitrogen prior to use. The aluminum reagents, methylaluminumoxane (MAO, 1.5 M in toluene) and modified methylaluminumoxane (MMAO, 2.5 M in *n*-heptane, containing 20–25%  $\text{Al}(i\text{-Bu})_3$ ), were purchased from Anhui Botai Electronic Materials Co. (Chuzhou, China), while high-purity ethylene was procured from Beijing Yanshan Petrochemical Co. (Beijing, China) and used as received. Other chemical reagents were purchased from Concord Technology Co., Ltd. (Tianjin, China), Macklin Biochemical Technology Co., Ltd. (Shanghai, China), and Innochem Technology Co., Ltd. (Beijing, China) and used as received: diethyl ether (GR., Concord, Tianjin, China), *n*-hexane (GR., Concord, Tianjin, China), glacial acetic acid (AR., Concord, Tianjin, China), *n*-butanol (AR., Concord, Tianjin, China), ferrous chloride tetrahydrate (98% purity, Macklin, Shanghai, China), anilines (99% purity, Innochem, Beijing, China). The samples for FT-IR analysis were placed directly on the ATR attachment plane and pressed with a flat nut, and the FT-IR spectra were recorded on a PerkinElmer System 2000 FT-IR spectrometer (PerkinElmer Scientific, Waltham, MA, USA). The elemental analyses were conducted using a Flash EA 1112 microanalyzer (Thermo Fisher Scientific, Waltham, MA, USA). The ESI mass spectra were recorded using a Bruker solariX instrument (Bruker Corporation, Billerica, MA, USA) (Acquisition Mode: Single MS; Polarity: Positive; Broadband Low Mass: 57.7  $m/z$ ; Acquired Scans: 20; Broadband

High Mass: 1000.0  $m/z$ ). The melting points of the polyethylenes were determined on a PerkinElmer TA-Q2000 DSC analyzer (PerkinElmer Scientific, Waltham, MA, USA) under a nitrogen atmosphere according to the following procedure: around 5.0 mg of the polymer was heated to 160 °C at a rate of 20 °C min<sup>-1</sup> and then maintained for 3 min at 160 °C to remove the thermal history. After cooling to -20 °C at a rate of 20 °C min<sup>-1</sup>, the sample was then heated to 160 °C again at the rate of 10 °C min<sup>-1</sup>. The polymer molecular weight ( $M_w$ ) and dispersity ( $M_w/M_n$ ) were measured using an Agilent PLGPC 220GPC system running (Agilent Technologies Inc., Santa Clara, CA, USA) at 150 °C using 1,2,4-trichlorobenzene as the mobile phase; sample preparation involved agitation of ca. 10 mg of the polyethylene sample in 1,2,4-trichlorobenzene (5 mL) at 170 °C for more than 8 h to allow dissolution. The <sup>1</sup>H NMR and <sup>13</sup>C NMR spectra of the polymers were measured at 100 °C using a Bruker AVANVE 500 MHz instrument (Bruker Corporation, Billerica, MA, USA); sample preparation involved dissolving the selected polyethylene (ca. 50 mg) in 1,1,2,2-tetrachloroethane-*d*<sub>2</sub> (0.6 mL), containing TMS as the internal standard, at 110 °C for more than 2 h. The 11-phenyl-1,2,3,7,8,9,10-heptahydrocyclohepta[*b*]quinoline-4,6-dione was prepared according to procedures reported elsewhere [29,39–41].

### 3.2. Synthesis of [*N,N*-diaryl-11-phenyl-1,2,3,7,8,9,10-heptahydrocyclohepta[*b*]quinoline-4,6-diimine] iron(II) Chloride (Fe1–Fe5)

#### 3.2.1. Aryl = 2,6-Dimethylphenyl (Fe1)

Under an atmosphere of nitrogen, a mixture of 11-phenyl-1,2,3,7,8,9,10-heptahydrocyclohepta[*b*]quinoline-4,6-dione (0.153 g, 0.50 mmol), 2,6-dimethylaniline (0.242 g, 2.0 mmol), and ferrous chloride tetrahydrate (0.080 g, 0.40 mmol) was dissolved in *n*-butanol (2.0 mL), containing a catalytic amount of acetic acid (0.5 mL), and then stirred and heated to reflux for 2 h to give a blue-green solution. After cooling to room temperature, diethyl ether and *n*-hexane (32 mL, v:v = 1:1) were added to induce precipitation. This precipitate was then left to settle, and the supernatant solution was discarded. This process of adding diethyl ether/*n*-hexane (32 mL, v:v = 1:1) and discarding the supernatant solution was repeated two more times. Finally, the mixture was filtered and washed three times with diethyl ether and *n*-hexane (24 mL, v:v = 2:1), affording **Fe1** as a blue powder (0.217, 85%). FT-IR (cm<sup>-1</sup>): 2950 (m), 1678 (m), 1617 (m,  $\nu_{C=N}$ ), 1570 (m), 1441 (s), 1376 (m), 1218 (s), 1073 (s), 920 (m), 844 (m), 770 (s), 704 (s). ESI-MS ( $m/z$ ): Calculated for [C<sub>36</sub>H<sub>37</sub>ClFeN<sub>3</sub>]<sup>+</sup> (602.20254). Found: 602.20232 (Figure S19). Elemental analysis: Calculated for C<sub>36</sub>H<sub>37</sub>Cl<sub>2</sub>N<sub>3</sub>Fe (638.46) C, 67.73, H, 5.84, N, 6.58. Found: C, 67.31, H, 6.25, N, 6.68%.

#### 3.2.2. Aryl = 2,6-Diethylphenyl (Fe2)

By using a similar procedure to that outlined for **Fe1**, but with 2,6-diethylaniline as the arylamine, **Fe2** was isolated as a blue powder (0.171 g, 66%). FT-IR (cm<sup>-1</sup>): 2965 (m), 2932 (m), 2870 (m), 1678 (m), 1613 (m,  $\nu_{C=N}$ ), 1567 (m), 1492 (m), 1447 (s), 1330 (m), 1216 (m), 1189 (m), 1106 (m), 1071 (m), 1030 (m), 951 (m), 848 (m), 809 (m), 776 (s), 703 (s). ESI-MS ( $m/z$ ): Calculated for [C<sub>40</sub>H<sub>45</sub>ClFeN<sub>3</sub>]<sup>+</sup> (658.26514). Found: 658.26496 (Figure S20). Elemental analysis: Calculated for C<sub>40</sub>H<sub>45</sub>Cl<sub>2</sub>N<sub>3</sub>Fe (694.57) C, 69.17, H, 6.53, N, 6.05. Found: C, 68.80, H, 6.71, N, 6.25%.

#### 3.2.3. Aryl = 2,6-Diisopropylphenyl (Fe3)

By using a similar procedure to that outlined for **Fe1**, but with 2,6-diisopropylaniline as the arylamine, **Fe3** was isolated as a blue powder (0.196 g, 65%). FT-IR (cm<sup>-1</sup>): 2962 (m), 2866 (m), 2361 (w), 1688 (w), 1611 (w,  $\nu_{C=N}$ ), 1568 (m), 1458 (s), 1383 (m), 1360 (m), 1324 (m), 1245 (m), 1214 (m), 1183 (m), 1124 (m), 1103 (m), 1051 (m), 943 (m), 848 (m), 804 (s), 774 (s), 709 (s). ESI-MS ( $m/z$ ): Calculated for [C<sub>44</sub>H<sub>53</sub>ClFeN<sub>3</sub>]<sup>+</sup> (714.32774). Found: 714.32762 (Figure S21). Elemental analysis: Calculated for C<sub>44</sub>H<sub>53</sub>Cl<sub>2</sub>N<sub>3</sub>Fe (750.67) C, 70.40, H, 7.12, N, 5.60. Found: C, 70.19, H, 7.42, N, 5.73%.

### 3.2.4. Aryl = 2,4,6-Trimethylphenyl (Fe4)

By using a similar procedure to that outlined for **Fe1**, but with 2,4,6-trimethylaniline as the arylamine, **Fe4** was isolated as a blue powder (0.232 g, 87%). ESI-MS ( $m/z$ ): Calculated for  $[\text{C}_{38}\text{H}_{41}\text{ClFeN}_3]^+$  (630.23384). Found: 630.23370 (Figure S22). FT-IR ( $\text{cm}^{-1}$ ): 3336 (m), 2912 (s), 2108 (w), 1984 (w), 1683 (w), 1604 (w,  $\nu_{\text{C}=\text{N}}$ ), 1561 (m), 1472 (s), 1440 (s), 1376 (m), 1325 (m), 1215 (s), 1148 (m), 1071 (m), 1033 (m), 952 (w), 853 (s), 780 (w), 757 (w), 702 (s). Elemental analysis: Calculated for  $\text{C}_{38}\text{H}_{41}\text{Cl}_2\text{N}_3\text{Fe}$  (666.51) C, 68.84, H, 6.20, N, 6.30. Found: C, 68.71, H, 6.55, N, 6.17%.

### 3.2.5. Aryl = 2,6-Diethyl-4-methylphenyl (Fe5)

By using a similar procedure to that outlined for **Fe1**, but with 2,6-diethyl-4-methylaniline as the arylamine, **Fe5** was isolated as a blue powder (0.106 g, 37%). ESI-MS ( $m/z$ ): Calculated for  $[\text{C}_{42}\text{H}_{49}\text{ClFeN}_3]^+$  (686.29644). Found: 686.29592 (Figure S23). FT-IR ( $\text{cm}^{-1}$ ): 3363 (m), 2964 (m), 2930 (m), 2870 (m), 1676 (w), 1612 (m,  $\nu_{\text{C}=\text{N}}$ ), 1566 (m), 1456 (s), 1373 (m), 1335 (m), 1257 (m), 1215 (m), 1150 (m), 1070 (m), 950 (m), 857 (s), 774 (m), 704 (s). Elemental analysis: Calculated for  $\text{C}_{42}\text{H}_{49}\text{Cl}_2\text{N}_3\text{Fe}$  (722.62) C, 69.81, H, 6.84, N, 5.82. Found: C, 69.57, H, 7.03, N, 5.61%.

## 3.3. Polymerization Studies

### 3.3.1. Ethylene Polymerization at 1 Atm Ethylene Pressure

A 250 mL Schlenk vessel, equipped with a stirrer bar, was loaded with **Fe4** (0.7 mg, 1.0  $\mu\text{mol}$ ), and the vessel was subjected to three cycles of evacuation and back-filling with nitrogen before the atmosphere was replaced with ethylene (1 atm). Freshly distilled toluene (30 mL) was then injected to dissolve the iron complex, and the mixture was stirred and heated to 60 °C. The activator (MAO or MMAO) was immediately injected via a syringe, and the run commenced. After 30 min, the supply of ethylene was stopped and the pressure within the Schlenk flask vented. The reaction mixture was then quenched with 10% hydrochloric acid in ethanol (30 mL). The polymer was washed with ethanol and dried under reduced pressure at 100 °C until it reached a constant weight.

### 3.3.2. Ethylene Polymerization at 5 Atm or 10 Atm Ethylene Pressure

A 250 mL stainless steel autoclave, fitted with a mechanical stirrer, an ethylene pressure control device, and a temperature controller, was employed for the higher-pressure (5 atm or 10 atm) ethylene polymerization evaluations. The autoclave was evacuated and back-filled with high-purity nitrogen (2 cycles) and then pressurized with 5 atm of ethylene to check the gas tightness. With the ethylene pressure returning to 1 atm, the iron precatalyst (1.0  $\mu\text{mol}$ ), pre-mixed with toluene (25 mL) in a Schlenk tube, was immediately injected into the autoclave. Any remaining iron complex was washed into the autoclave with more toluene (25 mL), and then a further volume of toluene (25 mL) was added. The required amount of activator (MAO or MMAO) and additional toluene (25 mL) were injected successively into the autoclave to take the total volume of solvent to 100 mL. The ethylene pressure was then set at either 5 atm or 10 atm, and the stirring immediately commenced. After the requisite reaction time, the ethylene gas supplying the reactor was stopped, and the autoclave was allowed to cool to room temperature by surrounding it with an ice/water bath. The reactor was then slowly vented, and the contents of the autoclave were quenched with a 5% hydrochloric ethanol solution (50 mL). Finally, the polymer was filtered, washed three times with ethanol (30 mL), and dried under reduced pressure at 100 °C until it reached a constant weight.

## 3.4. Single Crystal X-ray Diffraction Studies

X-ray diffraction studies were conducted on **Fe2** and **Fe3**, using single crystals of each iron complex that had been grown in the glove box by the slow diffusion of diethyl ether into a dichloromethane solution at ambient temperature. A crystal of each was selected and mounted on an XtaLAB Synergy R HyPix diffractometer (Rigaku Corporation, Tokyo, Japan)

incorporating graphite-monochromated Cu-K $\alpha$  radiation ( $\lambda = 1.54184 \text{ \AA}$ ) at 170(2) K for **Fe2** and 169.99(10) K for **Fe3**, and data collection commenced. Using Olex2, the structures were solved by employing the ShelXT structure solution program using intrinsic phasing and refined with the ShelXL refinement package using least squares minimization [42,43].

#### 4. Conclusions

In summary, a straightforward one-pot strategy has been successfully implemented to prepare five examples of iron(II) chloride complexes, **Fe1–Fe5**, bearing bis(imino)pyridines fused with six- and seven-membered carbocyclic rings and further appended with a *para*-phenyl group. All these iron complexes have been characterized via FT-IR spectroscopy, ESI mass spectrometry, elemental analysis, and, in the cases of **Fe2** and **Fe3**, by single crystal X-ray diffraction. On activation with MMAO or MAO, **Fe1–Fe5** exhibited extremely high activity, with a maximum of  $35.92 \times 10^6 \text{ g (PE) mol}^{-1} (\text{Fe}) \text{ h}^{-1}$  seen for **Fe4**/MAO operating at 60 °C. All catalysts generated highly linear polymers with varying levels of vinyl end-groups that were dependent on run temperature. Interestingly, analysis of  $^1\text{H}$  NMR spectra of the polymers revealed higher rates of  $\beta$ -H elimination at 60 °C for the MMAO-activated system and 70 °C for the MAO-activated system, highlighting the key role played by temperature in influencing the competition between  $\beta$ -H elimination and chain transfer to aluminum. Moreover, considerable control of the polymer molecular weight could be achieved with **Fe4** found to form low molecular weight polymer with narrow dispersity at high temperatures (70 or 80 °C), while higher molecular weight material was formed at lower run temperatures.

Perhaps more importantly, **Fe4**/MMAO exhibited outstanding thermal stability and was indeed superior to the non-phenyl substituted iron analog **E**/MMAO (Ar = 2,4,6-trimethylphenyl, M = Fe, Scheme 1), which is evidenced by the optimal run temperature of **Fe4**/MMAO being 60 °C (*cf.* 40 °C for **E**/MMAO) and activity of  $34.10 \times 10^6 \text{ g (PE) mol}^{-1} (\text{Fe}) \text{ h}^{-1}$  (*cf.*  $15.15 \times 10^6 \text{ g (PE) mol}^{-1} (\text{Fe}) \text{ h}^{-1}$  for **E**/MMAO). Given the remoteness of the *para*-phenyl group from the active iron center, it would seem unlikely that it has a direct steric influence on the active site, though an indirect effect by impacting on the flexibility/steric properties of the neighboring fused carbocycles and, in turn, the binding properties of the  $N',N,N''$ -ligand may be at play; an electronic effect cannot, however, be ruled out. More generally, these *para*-phenyl substituted carbocyclic-fused bis(imino)pyridine iron complexes exhibit excellent performance for ethylene polymerization when compared with a series of fused ring iron counterparts, including **D**<sub>2(n=2)</sub> and **D**<sub>2(n=3)</sub> (Figure 1), especially with respect to catalytic activity. As a similar effect on catalytic activity and molecular weight has been seen with their *para*-phenyl substituted cobalt counterparts (**G**, Figure 1), we aim in future work to further probe the generality of this structural variation in catalyst design.

**Supplementary Materials:** The following supporting information can be downloaded at: <https://www.mdpi.com/article/10.3390/catal14030213/s1>. Figure S1: (a) GPC traces for the polyethylenes generated using **Fe4**/MAO at different run temperatures and (b) plots of catalytic activity and polymer molecular weight as a function of run temperature; Figure S2: (a) GPC traces for the polyethylenes generated using **Fe4**/MAO at various Al:Fe molar ratios and (b) plots of catalytic activity and polymer molecular weight as a function of Al:Fe molar ratio; Figure S3: (a) GPC traces for the polyethylenes generated using **Fe4**/MAO over reaction time and (b) plots of catalytic activity and polymer molecular weight as a function of reaction time; Figure S4: (a) GPC traces for the polyethylenes generated using **Fe1–Fe5** under MAO activation and (b) a bar chart showing the effects of variation in *N*-aryl group in **Fe1–Fe5** on catalytic activity and polymer molecular weight; Figure S5:  $^1\text{H}$  NMR spectrum of the polyethylene produced using **Fe4**/MMAO operating at 70 °C (entry 4, Table 2); recorded at 100 °C in 1,1,2,2-tetrachloroethane-*d*<sub>2</sub>; Figure S6:  $^1\text{H}$  NMR spectrum of the polyethylene produced using **Fe4**/MMAO operating at 60 °C (entry 3, Table 2); recorded at 100 °C in 1,1,2,2-tetrachloroethane-*d*<sub>2</sub>; Figure S7:  $^1\text{H}$  NMR spectrum of the polyethylene produced using **Fe4**/MMAO operating at 50 °C (entry 2, Table 2); recorded at 100 °C in 1,1,2,2-tetrachloroethane-*d*<sub>2</sub>; Figure S8:  $^1\text{H}$  NMR spectrum of the polyethylene produced using **Fe4**/MMAO operating at 40 °C

(entry 1, Table 2); recorded at 100 °C in 1,1,2,2-tetrachloroethane-*d*<sub>2</sub>; Figure S9: <sup>1</sup>H NMR spectrum of the polyethylene produced using Fe4/MAO operating at 40 °C (entry 1, Table 3); recorded at 100 °C in 1,1,2,2-tetrachloroethane-*d*<sub>2</sub>; Figure S10: <sup>1</sup>H NMR spectrum of the polyethylene produced using Fe4/MAO operating at 50 °C (entry 2, Table 3); recorded at 100 °C in 1,1,2,2-tetrachloroethane-*d*<sub>2</sub>; Figure S11: <sup>1</sup>H NMR spectrum of the polyethylene produced using Fe4/MAO operating at 60 °C (entry 3, Table 3); recorded at 100 °C in 1,1,2,2-tetrachloroethane-*d*<sub>2</sub>; Figure S12: <sup>1</sup>H NMR spectrum of the polyethylene produced using Fe4/MAO operating at 70 °C (entry 4, Table 3); recorded at 100 °C in 1,1,2,2-tetrachloroethane-*d*<sub>2</sub>; Figure S13: <sup>1</sup>H NMR spectrum of the polyethylene produced using Fe4/MAO operating at 80 °C (entry 5, Table 3); recorded at 100 °C in 1,1,2,2-tetrachloroethane-*d*<sub>2</sub>; Table S1: Determining the molar ratios of *a* (chain A, unsaturated) to *b* (chain B, fully saturated) for the PE's produced using Fe4/MMAO at various temperatures; Table S2: Determining the molar ratios of *a* (chain A, unsaturated) to *b* (chain B, fully saturated) for the PE's produced using Fe4/MAO at various temperatures; Table S3: Crystal data and structure refinement for Fe2 and Fe3. Figure S14: FT-IR spectrum of Fe1. Figure S15: FT-IR spectrum of Fe2. Figure S16: FT-IR spectrum of Fe3. Figure S17: FT-IR spectrum of Fe4. Figure S18: FT-IR spectrum of Fe5. Figure S19: ESI-MS spectrum of Fe1. Figure S20: ESI-MS spectrum of Fe2. Figure S21: ESI-MS spectrum of Fe3. Figure S22: ESI-MS spectrum of Fe4. Figure S23: ESI-MS spectrum of Fe5. References [24,29,38,44] are cited in the Supplementary Materials.

**Author Contributions:** Y.W.: methodology, investigation, data curation, writing—original draft preparation, and writing—review and editing; Z.W.: methodology, validation, supervision, and writing—review and editing; Q.Z.: data curation; Y.M.: software; G.A.S.: visualization, writing—review and editing; Y.S.: X-ray diffraction; W.-H.S.: conceptualization, resources, supervision, funding acquisition, and writing—review and editing. All authors have read and agreed to the published version of the manuscript.

**Funding:** This research was funded by the National Natural Science Foundation of China (21871275).

**Data Availability Statement:** CCDC reference numbers 2325145–2325146 contain Supplementary crystallographic Information for Fe2 and Fe3, and the data presented in this study are available in this article.

**Acknowledgments:** G.A.S. thanks the Chinese Academy of Sciences for a President's International Fellowship for Visiting Scientists.

**Conflicts of Interest:** The authors declare no conflicts of interest.

## References

1. Small, B.L.; Brookhart, M.; Bennett, A.M.A. Highly Active Iron and Cobalt Catalysts for the Polymerization of Ethylene. *J. Am. Chem. Soc.* **1998**, *120*, 4049–4050. [[CrossRef](#)]
2. Britovsek, G.J.P.; Gibson, V.C.; McTavish, S.J.; Solan, G.A.; White, A.J.P.; Williams, D.J.; Britovsek, G.J.P.; Kimberley, B.S.; Maddox, P.J. Novel olefin polymerization catalysts based on iron and cobalt. *Chem. Commun.* **1998**, 849–850. [[CrossRef](#)]
3. Small, B.L.; Brookhart, M. Iron-Based Catalysts with Exceptionally High Activities and Selectivities for Oligomerization of Ethylene to Linear  $\alpha$ -Olefins. *J. Am. Chem. Soc.* **1998**, *120*, 7143–7144. [[CrossRef](#)]
4. Britovsek, G.J.P.; Mastroianni, S.; Solan, G.A.; Baugh, S.P.D.; Redshaw, C.; Gibson, V.C.; White, A.J.P.; Williams, D.J.; Elsegood, M.R.J. Oligomerisation of Ethylene by Bis(imino)pyridyliron and -cobalt Complexes. *Chem. Eur. J.* **2000**, *6*, 2221–2231. [[CrossRef](#)] [[PubMed](#)]
5. Wang, Z.; Solan, G.A.; Zhang, W.; Sun, W.-H. Carbocyclic-fused N,N,N-pincer ligands as ring-strain adjustable supports for iron and cobalt catalysts in ethylene oligo-/polymerization. *Coord. Chem. Rev.* **2018**, *363*, 92–108. [[CrossRef](#)]
6. Gibson, V.C.; Redshaw, C.; Solan, G.A. Bis(imino)pyridines: Surprisingly Reactive Ligands and a Gateway to New Families of Catalysts. *Chem. Rev.* **2007**, *107*, 1745–1776. [[CrossRef](#)]
7. Bianchini, C.; Giambastiani, G.; Luconi, L.; Meli, A. Olefin oligomerization, homopolymerization and copolymerization by late transition metals supported by (imino)pyridine ligands. *Coord. Chem. Rev.* **2010**, *254*, 431–455. [[CrossRef](#)]
8. Britovsek, G.J.P.; Bruce, M.; Gibson, V.C.; Kimberley, B.S.; Maddox, P.J.; Mastroianni, S.; McTavish, S.J.; Redshaw, C.; Solan, G.A.; Stromberg, S.; et al. Iron and Cobalt Ethylene Polymerization Catalysts Bearing 2,6-Bis(imino)Pyridyl Ligands: Synthesis, Structures, and Polymerization Studies. *J. Am. Chem. Soc.* **1999**, *121*, 8728–8740. [[CrossRef](#)]
9. Ittel, S.D.; Johnson, L.K.; Brookhart, M. Late-Metal Catalysts for Ethylene Homo- and Copolymerization. *Chem. Rev.* **2000**, *100*, 1169–1204. [[CrossRef](#)]
10. Gibson, V.C.; Solan, G.A. Olefin Oligomerizations and Polymerizations Catalyzed by Iron and Cobalt Complexes Bearing Bis(imino)pyridine Ligands. In *Catalysis without Precious Metals*; Bullock, R.M., Ed.; Wiley-VCH: Weinheim, Germany, 2010; pp. 111–141.

11. Gibson, V.C.; Solan, G.A. Iron-Based and Cobalt-Based Olefin Polymerisation Catalysts. In *Metal Catalysts in Olefin Polymerization*; Guan, Z., Ed.; Springer: Berlin/Heidelberg, Germany, 2009; pp. 107–158.
12. Sun, W.-H.; Jie, S.; Zhang, S.; Zhang, W.; Song, Y.; Ma, H. Iron Complexes Bearing 2-Imino-1,10-phenanthrolyl Ligands as Highly Active Catalysts for Ethylene Oligomerization. *Organometallics* **2006**, *25*, 666–677. [[CrossRef](#)]
13. Pelletier, J.D.A.; Champouret, Y.D.M.; Cadarso, J.; Clowes, L.; Gañete, M.; Singh, K.; Thanarajasingham, V.; Solan, G.A. Electronically variable imino-phenanthrolyl-cobalt complexes; synthesis, structures and ethylene oligomerisation studies. *J. Organomet. Chem.* **2006**, *691*, 4114–4123. [[CrossRef](#)]
14. Jie, S.; Zhang, S.; Sun, W.-H.; Kuang, X.; Liu, T.; Guo, J. Iron(II) complexes ligated by 2-imino-1,10-phenanthrolines: Preparation and catalytic behavior toward ethylene oligomerization. *J. Mol. Catal. A Chem.* **2007**, *269*, 85–96. [[CrossRef](#)]
15. Appukuttan, V.K.; Liu, Y.; Son, B.C.; Ha, C.-S.; Suh, H.; Kim, I. Iron and Cobalt Complexes of 2,3,7,8-Tetrahydroacridine-4,5(1H,6H)-diimine Sterically Modulated by Substituted Aryl Rings for the Selective Oligomerization to Polymerization of Ethylene. *Organometallics* **2011**, *30*, 2285–2294. [[CrossRef](#)]
16. Zhang, W.; Chai, W.; Sun, W.-H.; Hu, X.; Redshaw, C.; Hao, X. 2-(1-(Arylimino)ethyl)-8-arylimino-5,6,7-trihydroquinoline Iron(II) Chloride Complexes: Synthesis, Characterization, and Ethylene Polymerization Behavior. *Organometallics* **2012**, *31*, 5039–5048. [[CrossRef](#)]
17. Sun, W.-H.; Kong, S.; Chai, W.; Shiono, T.; Redshaw, C.; Hu, X.; Guo, C.; Hao, X. 2-(1-(Arylimino)ethyl)-8-arylimino-5,6,7-trihydroquinolylcobalt dichloride: Synthesis and polyethylene wax formation. *Appl. Catal. A Gen.* **2012**, *447–448*, 67–73. [[CrossRef](#)]
18. Zhang, Y.; Suo, H.; Huang, F.; Liang, T.; Hu, X.; Sun, W.H. Thermo-stable 2-(arylimino)benzylidene-9-arylimino-5,6,7,8-tetrahydro cyclohepta[b]pyridyliron(II) precatalysts toward ethylene polymerization and highly linear polyethylenes. *J. Polym. Sci. Part A Polym. Chem.* **2016**, *55*, 830–842. [[CrossRef](#)]
19. Du, S.; Zhang, W.; Yue, E.; Huang, F.; Liang, T.; Sun, W.H.  $\alpha, \alpha'$ -Bis(arylimino)-2,3:5,6-bis(pentamethylene)pyridylcobalt Chlorides: Synthesis, Characterization, and Ethylene Polymerization Behavior. *Eur. J. Inorg. Chem.* **2016**, *2016*, 1748–1755. [[CrossRef](#)]
20. Du, S.; Wang, X.; Zhang, W.; Flisak, Z.; Sun, Y.; Sun, W.-H. A practical ethylene polymerization for vinyl-polyethylenes: Synthesis, characterization and catalytic behavior of  $\alpha, \alpha'$ -bisimino-2,3:5,6-bis(pentamethylene)pyridyliron chlorides. *Polym. Chem.* **2016**, *7*, 4188–4197. [[CrossRef](#)]
21. Wang, Z.; Solan, G.A.; Mahmood, Q.; Liu, Q.; Ma, Y.; Hao, X.; Sun, W.-H. Bis(imino)pyridines Incorporating Doubly Fused Eight-Membered Rings as Conformationally Flexible Supports for Cobalt Ethylene Polymerization Catalysts. *Organometallics* **2018**, *37*, 380–389. [[CrossRef](#)]
22. Wang, Z.; Zhang, R.; Zhang, W.; Solan, G.A.; Liu, Q.; Liang, T.; Sun, W.-H. Enhancing thermostability of iron ethylene polymerization catalysts through N,N,N-chelation of doubly fused  $\alpha, \alpha'$ -bis(arylimino)-2,3:5,6-bis(hexamethylene)pyridines. *Catal. Sci. Technol.* **2019**, *9*, 1933–1943. [[CrossRef](#)]
23. Wang, Z.; Ma, Y.; Guo, J.; Liu, Q.; Solan, G.A.; Liang, T.; Sun, W.-H. Bis(imino)pyridines fused with 6- and 7-membered carbocyclic rings as N,N,N-scaffolds for cobalt ethylene polymerization catalysts. *Dalton Trans.* **2019**, *48*, 2582–2591. [[CrossRef](#)] [[PubMed](#)]
24. Wang, Z.; Solan, G.A.; Ma, Y.; Liu, Q.; Liang, T.; Sun, W.-H. Fusing Carbocycles of Inequivalent Ring Size to a Bis(imino)pyridine-Iron Ethylene Polymerization Catalyst: Distinctive Effects on Activity, PE Molecular Weight, and Dispersity. *Research* **2019**, *2019*, 9426063. [[CrossRef](#)] [[PubMed](#)]
25. Mazzolini, J.; Boyron, O.; Monteil, V.; Gignes, D.; Bertin, D.; D'Agosto, F.; Boisson, C. Polyethylene End Functionalization Using Radical-Mediated Thiol–Ene Chemistry: Use of Polyethylenes Containing Alkene End Functionality. *Macromolecules* **2011**, *44*, 3381–3387. [[CrossRef](#)]
26. Wang, X.; Nozaki, K. Selective Chain-End Functionalization of Polar Polyethylenes: Orthogonal Reactivity of Carbene and Polar Vinyl Monomers in Their Copolymerization with Ethylene. *J. Am. Chem. Soc.* **2018**, *140*, 15635–15640. [[CrossRef](#)] [[PubMed](#)]
27. Amin, S.B.; Marks, T.J. Versatile Pathways for In Situ Polyolefin Functionalization with Heteroatoms: Catalytic Chain Transfer. *Angew. Chem. Int. Ed.* **2008**, *47*, 2006–2025. [[CrossRef](#)] [[PubMed](#)]
28. Cámpora, J.; Naz, A.M.; Palma, P.; Rodríguez-Delgado, A.; Álvarez, E.; Tritto, I.; Boggioni, L. Iron and Cobalt Complexes of 4-Alkyl-2,6-diiminopyridine Ligands: Synthesis and Ethylene Polymerization Catalysis. *Eur. J. Inorg. Chem.* **2008**, *2008*, 1871–1879. [[CrossRef](#)]
29. Wang, Y.; Wang, Z.; Zhang, Q.; Zou, S.; Ma, Y.; Solan, G.A.; Zhang, W.; Sun, W.-H. Exploring Long Range para-Phenyl Effects in Unsymmetrically Fused bis(imino)pyridine-Cobalt Ethylene Polymerization Catalysts. *Catalysts* **2023**, *13*, 1387. [[CrossRef](#)]
30. Zhang, Q.; Yang, W.; Wang, Z.; Solan, G.A.; Liang, T.; Sun, W.-H. Doubly fused N,N,N-iron ethylene polymerization catalysts appended with fluoride substituents; probing catalytic performance via a combined experimental and MLR study. *Catal. Sci. Technol.* **2021**, *11*, 4605–4618. [[CrossRef](#)]
31. Masuda, J.D.; Wei, P.; Stephan, D.W. Nickel and palladium phosphinimine-imine ligand complexes. *Dalton Trans.* **2003**, *18*, 3500–3505. [[CrossRef](#)]
32. Addison, A.W.; Rao, T.N. Synthesis, structure, and spectroscopic properties of copper(II) compounds containing nitrogen–sulphur donor ligands; the crystal and molecular structure of aqua[1,7-bis(N-methylbenzimidazol-2'-yl)-2,6-dithiaheptane]copper(II) perchlorate. *J. Chem. Soc. Dalton Trans.* **1984**, 1349–1356. [[CrossRef](#)]

33. Long, Z.; Wu, B.; Yang, P.; Li, G.; Liu, Y.; Yang, X.-J. Synthesis and characterization of para-nitro substituted 2,6-bis(phenylimino)pyridyl Fe(II) and Co(II) complexes and their ethylene polymerization properties. *J. Organomet. Chem.* **2009**, *694*, 3793–3799. [[CrossRef](#)]
34. Guo, L.; Gao, H.; Zhang, L.; Zhu, F.; Wu, Q. An Unsymmetrical Iron(II) Bis(imino)pyridyl Catalyst for Ethylene Polymerization: Effect of a Bulky Ortho Substituent on the Thermostability and Molecular Weight of Polyethylene. *Organometallics* **2010**, *29*, 2118–2125. [[CrossRef](#)]
35. Liu, T.; Ma, Y.; Solan, G.A.; Sun, Y.; Sun, W.-H. Unimodal polyethylenes of high linearity and narrow dispersity by using ortho-4,4'-dichlorobenzhydryl-modified bis(imino)pyridyl-iron catalysts. *New J. Chem.* **2023**, *47*, 5786–5795. [[CrossRef](#)]
36. Bianchini, C.; Giambastiani, G.; Rios, I.G.; Mantovani, G.; Meli, A.; Segarra, A.M. Ethylene oligomerization, homopolymerization and copolymerization by iron and cobalt catalysts with 2,6-(bis-organylimino)pyridyl ligands. *Coord. Chem. Rev.* **2006**, *250*, 1391–1418. [[CrossRef](#)]
37. Han, M.; Oleynik, I.I.; Liu, M.; Ma, Y.; Oleynik, I.V.; Solan, G.A.; Liang, T.; Sun, W.H. Ring size enlargement in an ortho-cycloalkyl-substituted bis(imino)pyridine-cobalt ethylene polymerization catalyst and its impact on performance and polymer properties. *Appl. Organomet. Chem.* **2022**, *36*, e6529. [[CrossRef](#)]
38. Zhang, Q.; Zuo, Z.; Ma, Y.; Liang, T.; Yang, X.; Sun, W.-H. Fluorinated 2,6-bis(arylimino)pyridyl iron complexes targeting bimodal dispersive polyethylenes: Probing chain termination pathways via a combined experimental and DFT study. *Dalton Trans.* **2022**, *51*, 8290–8302. [[CrossRef](#)] [[PubMed](#)]
39. Dabiri, M.; Baghbanzadeh, M.; Nikcheh, M.S. Oxalic Acid: An Efficient and Cost-Effective Organic Catalyst for the Friedländer Quinoline Synthesis under Solvent-Free Conditions. *Monatsh. Chem.* **2007**, *138*, 1249–1252. [[CrossRef](#)]
40. Bell, T.W.; Khasanov, A.B.; Drew, M.G.B. Role of Pyridine Hydrogen-Bonding Sites in Recognition of Basic Amino Acid Side Chains. *J. Am. Chem. Soc.* **2002**, *124*, 14092–14103. [[CrossRef](#)]
41. Vierhapper, F.W.; Eliel, E.L. Selective Hydrogenation of Quinoline and Its Homologs, Isoquinoline, and Phenyl-Substituted Pyridines in the Benzene Ring. *J. Org. Chem. Vol.* **1975**, *40*, 2729–2734. [[CrossRef](#)]
42. Sheldrick, G.M. Crystal structure refinement with SHELXL. *Acta Crystallogr. C* **2015**, *71*, 3–8. [[CrossRef](#)]
43. Sheldrick, G. SHELXT—Integrated space-group and crystal-structure determination. *Acta Crystallogr. A* **2015**, *71*, 3–8. [[CrossRef](#)]
44. Fulmer, G.R.; Miller, A.J.M.; Sherden, N.H.; Gottlieb, H.E.; Nudelman, A.; Stoltz, B.M.; Bercaw, J.E.; Goldberg, K.I. NMR Chemical Shifts of Trace Impurities: Common Laboratory Solvents, Organics, and Gases in Deuterated Solvents Relevant to the Organometallic Chemist. *Organometallics* **2010**, *29*, 2176–2179. [[CrossRef](#)]

**Disclaimer/Publisher's Note:** The statements, opinions and data contained in all publications are solely those of the individual author(s) and contributor(s) and not of MDPI and/or the editor(s). MDPI and/or the editor(s) disclaim responsibility for any injury to people or property resulting from any ideas, methods, instructions or products referred to in the content.